Dual-mode dual-band bandpass filter design utilising cylindrical TM-mode cavities

Chad Bartlett✉ and Michael Höft
Institute of Electrical and Information Technology, Chair of Microwave Engineering, University of Kiel, Kiel, Germany
✉Email: chb@tf.uni-kiel.de

This letter presents the design of a novel dual-mode dual-band bandpass filter that utilises the TM210 and TM020 modes of cylindrical cavity resonators for millimetre-wave operation when fed with standard WR-10 waveguide ports. In this manner, the two selected modes of the cylindrical cavity resonators are demonstrated as a single propagation path for fixed dual-passband responses without the need of cavity perturbations or tuning screws. The passbands are designated for centre frequencies at approximately 102.8 and 110.9 GHz and exhibit a four-pole Chebyshev characteristic in each of the passbands, which are separated by a transmission zero location. Simulated and measured results of the prototype are presented to verify the design.

Introduction: With an ever-increasing demand on wireless communication systems, methods for increasing the capacity of satellite and terrestrial communications systems have required successive advancements in regard to design schemes as well as novel technologies. To overcome many of the stringent requirements that are imposed by manufacturers, multi-band systems have been proposed as a viable solution because of their inherent compact size and lowered material cost. Although these multi-band systems have been demonstrated in a variety of technologies, standard rectangular and circular waveguide technologies have been on the forefront of high-frequency applications due to superior characteristics such as high quality factor, low loss and high power handling [1–4].

As trends continue for the allocation of high-frequency bands well into the terahertz and sub-terahertz regions, multi-band designs depend on continuous filter developments in order to achieve these innovative demands. To the best of the authors' knowledge, only a few dual-band bandpass filters (DBBPFs) have been demonstrated in the WR-3 and WR-10 bands [5–9]. Each of these designs has been able to demonstrate notable results by taking advantage of multiple paths through the waveguide or by splitting a broad passband into dual sub-bands. In this letter, we seek to demonstrate a novel dual-mode dual-band filter that is based on the concepts introduced in [10–12], which exploits the TM210 and TM020 modes in each of the filter's resonator cavities. In this manner, a DBBPF devised of unperturbed cylindrical cavity resonators is presented in single-path operation by taking advantage of the passband locations that are determined by the resonance of each mode; the two distinct modes share commonality of the resonator shape and, therefore, provide predictable and fixed bandpass locations that can be exploited in high-frequency designs where tuning-means become difficult or impractical to implement. To this end, the design demonstrates a four-pole Chebyshev filtering characteristic in the upper W-band and lower D-band through a dual-mode resonator path, which is fed by standard WR-10 waveguide ports. The prototype is designed and manufactured for centre frequencies at approximately 102.8 and 110.9 GHz, effectively taking advantage of the larger dimensions to support both frequencies of operation. Along with maintaining narrow passband bandwidths of approximately 1%, the use of the higher mode resonators in waveguide technology allows for a low insertion loss to be obtained in each of the passbands.

Filter design: For the design of the filter structure, cylindrical cavities are selected for their TM-mode properties and are connected to rectangular waveguide input/output sections. Many other designs with similar interconnecting waveguide structures have been able to demonstrate good results in the literature for single- or multi-band use in this manner, several examples being [2–4,11–19], where in contrast to most, this filter utilises cylindrical resonators to create dual-passbands within common resonator dimensions without the need for tuning screws or perturbations within the cavities. The use of these types of larger cavities is favourable not only for their higher quality factor, but also for their larger and less restrictive dimensions during the milling procedure.

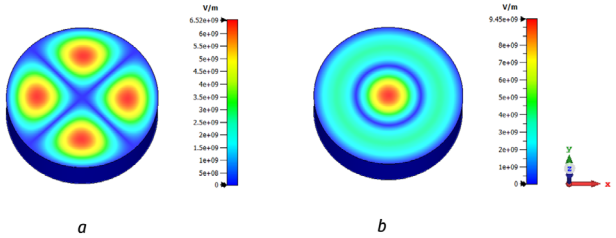

Fig. 1 *Distribution of the electric fields in the described cylindrical resonator. (a) Magnitude of the TM210 mode electric field. (b) Magnitude of the TM020 mode electric field*

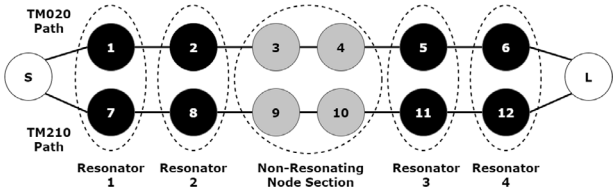

Fig. 2 *Topology path of the filter with extension to handle dual-band NRNs. Resonating nodes are black, source/load nodes are white and NRNs are grey*

For the design of a cylindrical cavity resonator, the resonant frequencies and initial dimensions can be found from

$$\frac{c}{2\pi\sqrt{\mu_r\epsilon_r}}\sqrt{\left(\frac{p_{nm}}{a}\right)^2+\left(\frac{l\pi}{d}\right)^2} \tag{1}$$

of [20] for each mode, where c is the speed of light, μ_r is the relative permeability, ε_r is the relative permittivity, n, m and l are the mode numbers, p_{nm} is a table coefficient determined from [20], and a and d are the radius and height of the cavity, respectively. Modelling of the cavity in CST Microwave Studio's eigenmode solver helps to discern the desirable field distributions for possible filter operation. For the case at hand, a cavity with a radius of 2.35 mm and height of 1.27 mm is selected for its TM210 and TM020 mode properties. As the selected TM modes are related only to the radius of the cylindrical cavities, the height of 1.27 mm was selected to match the milling depth of standard WR-10 waveguides. Figure 1 depicts the electric field distributions of both of these modes within the desired cavity.

In order to utilise the cylindrical resonators in a higher-order design, we cascade the filter in the same manner as [10–12] by utilising a non-resonating node (NRN) section as an interconnect between the second and third resonators. Figure 2 demonstrates the topology of dual-mode paths through the filter, which is comprised of a dual NRN section, where each of the modes is sharing a quarter-wavelength inverter path. This, in turn, also effects the definition of the coupling matrix, which must be extended to handle NRN's in the diagonal column for M_{33} and M_{44}, as discussed by Amari and Rosenberg [10]. The quarter-wavelength inverter between the NRN's is set to unity ($M_{34} = 1$) for convenience in the same manner as [10–12]. This section is first defined for a centre frequency of 106.85 GHz (the centre of the two passbands). Since there is loading effects from the cylindrical resonators to the NRN section, the slot is extended and, therefore, acts as a quarter-wave inverter section for each of the passbands. A 3-D view and the corresponding dimensions of the filter are shown in Figure 3. A general coupling matrix can be formulated as

$$\begin{bmatrix} 0 & M_{S1} & 0 & 0 & 0 & 0 & 0 & 0 \\ M_{S1} & 0 & M_{12} & 0 & 0 & 0 & 0 & 0 \\ 0 & M_{12} & 0 & M_{23} & 0 & 0 & 0 & 0 \\ 0 & 0 & M_{23} & 0 & M_{34} & 0 & 0 & 0 \\ 0 & 0 & 0 & M_{34} & 0 & M_{45} & 0 & 0 \\ 0 & 0 & 0 & 0 & M_{45} & 0 & M_{56} & 0 \\ 0 & 0 & 0 & 0 & 0 & M_{56} & 0 & M_{6L} \\ 0 & 0 & 0 & 0 & 0 & 0 & M_{6L} & 0 \end{bmatrix} \tag{2}$$

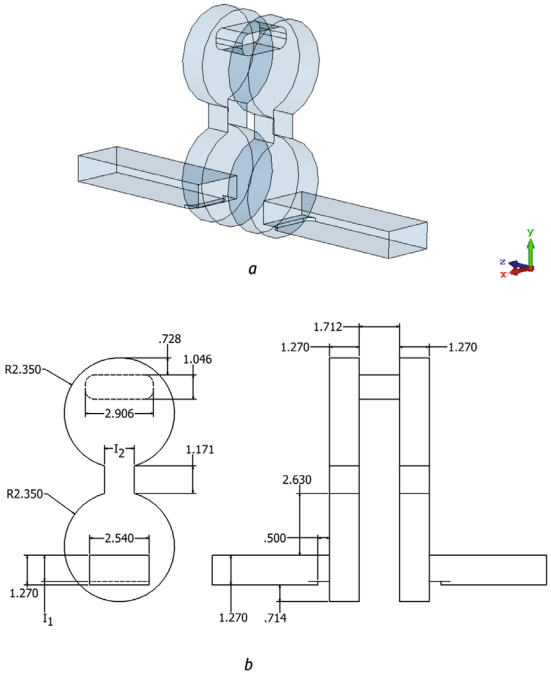

Fig. 3 *Configuration of the dual-mode dual-band filter. (a) Perspective view of the filter's vacuum shell. (b) Basic filter dimensions in (mm); values are rounded to three decimal places*

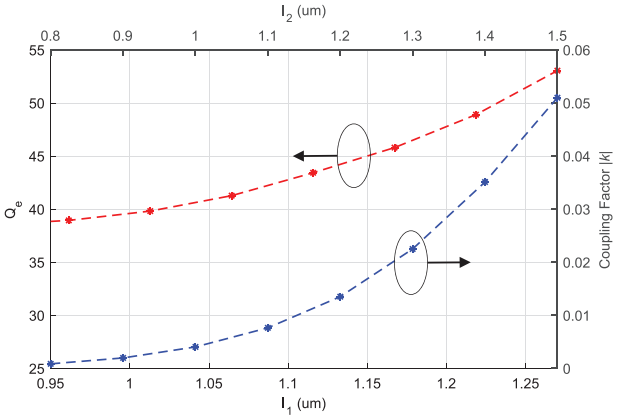

Fig. 4 *Dependence of the external quality factor* Q_e *and coupling value* k *on iris size* I_1 *and* I_2*, respectively. The red line corresponds to the external quality factor* Q_e *value, while the blue line corresponds to the coupling factor* k

where $M_{S1} = M_{6L} = 1.1497$, $M_{12} = M_{56} = 1.0369$, $M_{23} = M_{45} = 0.8767$ and $M_{34} = 1$, using the following dual-mode dual-band equations:

$$|k| = \frac{f_2^2 f_4^2 - f_1^2 f_3^2}{f_2^2 f_4^2 + f_1^2 f_3^2} \tag{3}$$

$$\Omega = \gamma \frac{(\omega^2 - \omega_1^2)(\omega^2 - \omega_2^2)}{\omega^2(\omega^2 - \omega_m^2)} \tag{4}$$

$$\frac{1}{Q_e} = \frac{1}{Q_{e1}} + \frac{1}{Q_{e2}} \tag{5a}$$

$$Q_e = \frac{\gamma}{M_{S1}^2} \tag{5b}$$

as presented in [21], where the coupling coefficient k takes the form of (3), the frequency transformation as (4), and the external quality factor as (5), where f_1, f_2, f_3 and f_4 are the resonate peaks of two coupled dual-mode dual-band resonators, $Q_e = 43.12$, $\gamma = 57$, $\omega_1 = 2\pi \cdot 102.82$ GHz, $\omega_2 = 2\pi \cdot 110.9$ GHz, $\omega_m = 2\pi \cdot 107.337$ GHz, and Q_{en} for $n = 1,2$ are the external quality factors of each mode. Figure 4 demonstrates the effect of changing iris dimensions I_1 and I_2, as defined in Figure 3(b), for the external quality factor Q_e and coupling factor k, respectively. For this design, $I_1 = 1.113$ mm and $I_2 = 1.257$ mm. An interesting point in regard to the coupling matrix values M_{23} and M_{45} (the coupling between

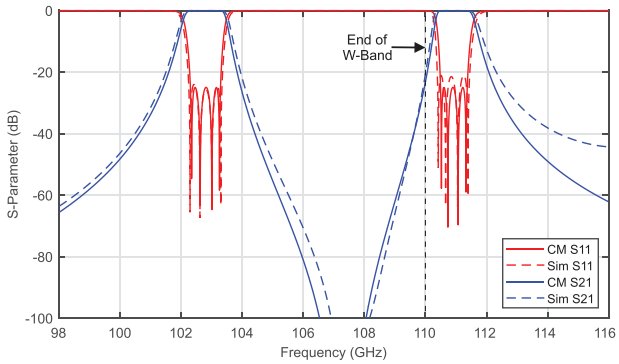

Fig. 5 *Simulated lossless* S*-parameters versus coupling matrix (2) of the proposed dual-mode dual-band filter*

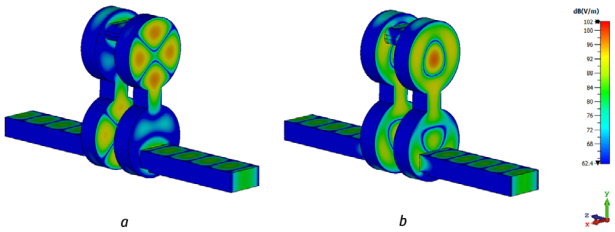

Fig. 6 *Three-dimensional views of the dual-mode dual-band filter structure with depictions of the simulated electric field interactions; the magnitude of each electric field is shown at the centre frequency of each passband. (a) Interaction of the TM210 mode. (b) Interaction of the TM020 mode*

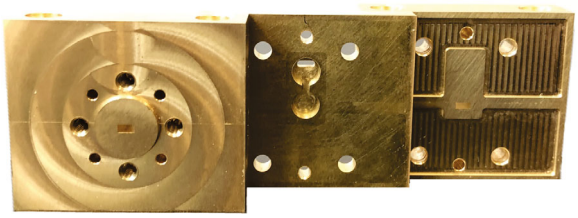

Fig. 7 *Manufactured prototype in brass (disassembled)*

resonators 2 and 3 to the NRN section) is that by disconnecting resonator 2 (and similarly for 3) at the inverter, and treating the resonator as an external quality factor calculation (5), we compute a value of $M_{23} = 0.8870$, which is very close to the coupling goal $M_{23} = 0.8767$ required from (2).

A comparison is made in Figure 5 between the lossless simulated results and coupling matrix profile of (2) over the range of 98–116 GHz. The lossless simulated response of each passband demonstrates a return loss that is better than 20 dB and has corresponding bandwidths of approximately 1%. The centre frequency of the first band is located at approximately 102.8 GHz, the upper end of the W-band, while the second band is located at the lowest end of the D-band and centred at approximately 110.9 GHz. Simulation of the TM210 and TM020 modes within the filter is depicted in Figure 6. These images serve as a visual representation of the electric field interactions (in magnitude) throughout the structure.

Manufacturing and results: For the manufacture of the structure in waveguide technology, the filter is split into five separate blocks to be milled by CNC (computer numerical control). The given dimensions of the cascaded structure are defined in Figure 3(b), while the milling radius is designated as 0.4 mm. It can be noted that the use of the WR-10 waveguide input/output ports allows us to designate a passband response in the lower D-band while still taking advantage of the WR-10 waveguide's larger and less restrictive dimensions. Although this technique is well known in industry, it remains as a suitable method of overcoming manufacturing issues in very high frequency components.

Brass has been selected as the cutting material due to machinability and final surface finish. Figure 7 depicts the manufactured pieces before final assembly. The brass component shown in the centre of Figure 7 houses each of the four main resonator cavities on either side of the

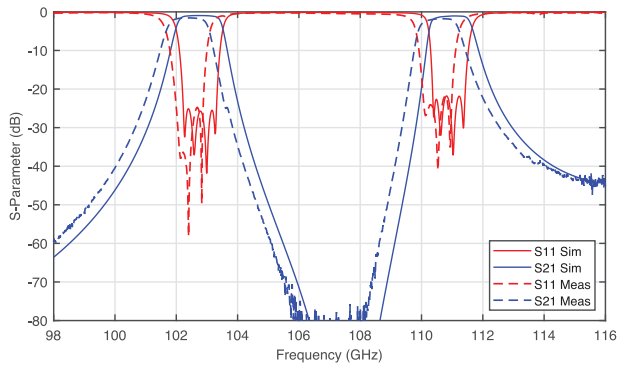

Fig. 8 *Simulated versus measured* S*-parameters of the dual-mode dual-band filter*

Table 1. Comparison of dual-band WR-10 waveguide filters in the literature

Refer.	Centre Freq. (GHz)	Filter Path Layout	Tech.	Min in-band IL (dB)	RL* (dB)	Filter Type
[8]	80.0/100.0	Dual	CNC	1.36/1.50	>20/19	Quasi-elliptic
[9]	85.35/101.45	Dual	CNC	1.02/2.05	>20/20	Cheb.
This work	102.8/110.9	Single	CNC	1.57/1.80	>20/20	Cheb.

*Estimated values at measured centre frequencies.

structure, while the NRN section is milled through the block to connect resonators 2 and 3. The other brass pieces shown act to enclose the resonator cavities of the centre brass section as well as house the input/output waveguides and their associated irises. Once assembled, the filter is tested using a Rohde & Schwarz ZVA67 with W-band up-converters.

Figure 8 presents a comparison of the simulated and measured results of the WR-10 dual-mode dual-band filter over 98–116 GHz. This direct comparison demonstrates good measured results over the entire frequency region of interest. The measured return loss is better than 20 dB in both the first and second passbands. A small shift in centre frequency can be observed, which has pushed both passbands to slightly lower frequencies. The simulated insertion losses at the centre frequencies of the lower and upper passbands are better than 0.96 and 1.12 dB, respectively, when the conductivity of brass is taken as 1.59e+07 S/m. The measured insertion loss values reach approximately 1.57 and 1.8 dB for the lower and upper passbands, respectively, which is less than 1 dB of loss at each of the centre passbands when compared with the simulated results. Although the simulated conductivity of brass is viewed as an overvaluation, additional losses can be attributed to the final-milled surface roughness as well as any misalignment or gaps between each of the five brass parts after assembly. Table 1 is provided as a general comparison of dual-band WR-10 waveguide filters that have been proposed in the literature. Although this design utilises the fixed frequencies based on the modes of a shared resonator size and path, the measured results are quite similar to the achievements presented in [8] and [9].

Conclusion: A new dual-mode dual-band passband filter that utilises the TM210 and TM020 modes of cylindrical resonators has been presented for operation in the upper W-band and lower D-band, where, in this manner, the shared resonator size and selected modes allow the designer to use fixed and predictable centre frequency locations. A discussion on the design approach and coupling matrix profile has been presented. The prototype has been manufactured as five separate brass pieces and tested in the laboratory. Measurements of the filter have shown a return loss that is better than 20 dB and insertion loss better than 1.8 dB in each of the passbands. The measured results agree well with the proposed filter simulations, thus allowing for the design approach to be verified. A table outlining the existing dual-band WR-10 waveguide filters in the literature has been presented for comparison of general characteristics. This work provides a progressive step for the implementation of higher-order cylindrical cavities at millimetre-wave frequencies without the use of tuning screws or cavity perturbations.

Acknowledgement: This work was supported by the European Union's Horizon 2020 research and innovation programme under Marie Skłodowska-Curie grant agreement 811232-H2020-MSCA- ITN-2018. The authors would also like to acknowledge Dr. Hans-Ulrich Nickel of Spinner GmbH for his thoughtful advice and help with laboratory measurements.

Open access funding enabled and organized by Projekt DEAL.

Received: *30 December 2020* Accepted: *10 February 2021*
doi: 10.1049/ell2.12127

References

1 Amari, S., Bekheit, M.: A new class of dual-mode dual-band waveguide filters. *IEEE Trans. Microwave Theory Tech.* **56**(8), 1938–1944 (2008)
2 Zhu, L., Mansour, R.R., Yu, M.: Quasi-elliptic waveguide dual-band bandpass filters. *IEEE Trans. Microwave Theory Tech.*, **67**(12), 5029–5037 (2019)
3 Nocella, V., et al.: Dual-band filters based on TM dual-mode cavities. In: 44th European Microwave Conference, 2014, pp. 179–182
4 Naeem, U., Perigaud, A., Bila, S.: Dual-mode dual-band bandpass cavity filters with widely separated passbands. *IEEE Trans. Microwave Theory Tech.* **65**(8), 2681–2686 (2017)
5 Huang, Y., et al.: WR-3 dual-band bandpass filter based on parallel coupling structure. *Microsyst. Tech.* **23**(7), 2553–2559 (2017)
6 Shang, X., et al.: WR-3 band waveguides and filters fabricated using SU8 photoresist micromachining technology. *IEEE Trans. THz Sci. Technol.* **2**(6), 629–637 (2012)
7 Cao, X., Tang, Z., Bao, J.: Design of a dual-band waveguide filter based on micromachining fabrication process. *IET Microwave Antennas Propag.* **10**(4), 459–463 (2016)
8 Zhou, K., et al.: W-band dual-band quasi-elliptical waveguide filter with flexibly allocated frequency and bandwidth ratios. *IEEE Microwave Wireless Compon. Lett.*, **28**(3), 206–208 (2018)
9 Chen, J., et al.: W-band dual-band waveguide band-pass filter using dual-mode cavities. *Electron. Lett.* **54**(25), 1444–1446 (2018)
10 Amari, S., Rosenberg, U.: New building blocks for modular design of elliptic and self-equalized filters. *IEEE Trans. Microwave Theory Tech.* **52**(2), 721–736 (2004)
11 Bastioli, S., Tomassoni, C., Sorrentino, R.: A new class of waveguide dual-mode filters using TM and nonresonating modes. *IEEE Trans. Microwave Theory Tech.* **58**(12), 3909–3917 (2010)
12 Tomassoni, C., Bastioli, S., Sorrentino, R.: Generalized TM dual-mode cavity filters. *IEEE Trans. Microwave Theory Tech.* **59**(12), 3338–3346 (2011)
13 Glubokov, O., et al.: Micromachined filters at 450 GHz with 1% fractional bandwidth and unloaded Q beyond 700. *IEEE Trans. THz Sci. Technol.* **9**(1), 106–108 (2018)
14 Shang, X., Lancaster, M., Dong, Y.-L.: W-band waveguide filter based on large TM120 resonators to ease CNC milling. *Electron. Lett.* **53**(7), 488–490 (2017)
15 Lee, J., Uhm, M.S., Yom, I.B.: A dual-passband filter of canonical structure for satellite applications. *IEEE Microwave Wireless Compon. Lett.*, **14**(6), 271–273 (2004)
16 Zhu, L., Mansour, R.R., Yu, M.: A compact waveguide quasi-elliptic dual-band filter. In: IEEE MTT-S Int. Microwave Symposium Digest, 2019, pp. 1179–1182
17 Naeem, U., et al.: A dual-band bandpass filter with widely separated passbands. *IEEE Trans. Microwave Theory Tech.* **62**(3), 450–456 (2014)
18 Lenoir, P., et al.: Synthesis and design of asymmetrical dual-band bandpass filters based on equivalent network simplification. *IEEE Trans. Microwave Theory Tech.* **54**(7), 3090–3097 (2006)
19 Liu, M., et al.: Design of 4th order cylindrical filter suitable for SU-8 micromachining. In: IEEE MTT-S International Microwave Workshop Series on Advanced Materials and Processes for RF and THz Applications, 2020, pp. 1–3
20 Pozar, D.M.: *Microwave engineering*, 4th ed. Wiley, Hoboken, NJ, 2009
21 Ma, P., et al.: A design method of multimode multiband bandpass filters. *IEEE Trans. Microwave Theory Tech.* **66**(6), 2791–2799 (2018)